Mechanism of Coenzyme Binding to Human Methionine Synthase Reductase Revealed through the Crystal Structure of the FNR-like Module and Isothermal Titration Calorimetry † , ‡

ARTICLE *in* BIOCHEMISTRY · NOVEMBER 2007

Impact Factor: 3.02 · DOI: 10.1021/bi701209p · Source: PubMed

Mechanism of Coenzyme Binding to Human Methionine Synthase Reductase Revealed through the Crystal Structure of the FNR-like Module and Isothermal Titration Calorimetry[†,‡]

Kirsten R. Wolthers, Xiaodong Lou, Helen S. Toogood, David Leys, and Nigel S. Scrutton*

Faculty of Life Sciences, University of Manchester, Manchester Interdisciplinary Biocentre, 131 Princess Street, Manchester M1 7DN, United Kingdom

Received June 19, 2007; Revised Manuscript Received August 15, 2007

ABSTRACT: Human methionine synthase reductase (MSR) is a 78 kDa flavoprotein that regenerates the active form of cobalamin-dependent methionine synthase (MS). MSR contains one FAD and one FMN cofactor per polypeptide and functions in the sequential transfer of reducing equivalents from NADPH to MS via its flavin centers. We report the 1.9 Å crystal structure of the $NADP^+$-bound FNR-like module of MSR that spans the NADP(H)-binding domain, the FAD-binding domain, the connecting domain, and part of the extended hinge region, a feature unique to MSR. The overall fold of the protein is similar to that of the corresponding domains of the related diflavin reductase enzymes cytochrome P450 reductase and neuronal nitric oxide synthase (NOS). However, the extended hinge region of MSR, which is positioned between the NADP(H)/FAD- and FMN-binding domains, is in an unexpected orientation with potential implications for the mechanism of electron transfer. Compared with related flavoproteins, there is structural variation in the NADP(H)-binding site, in particular regarding those residues that interact with the 2′-phosphate and the pyrophosphate moiety of the coenzyme. The lack of a conserved binding determinant for the 2′-phosphate does not weaken the coenzyme specificity for NADP(H) over NAD(H), which is within the range expected for the diflavin oxidoreductase family of enzymes. Isothermal titration calorimetry reveals a binding constant of 37 and 2 μM for binding of $NADP^+$ and 2′,5′-ADP, respectively, for the ligand−protein complex formed with full-length MSR or the isolated FNR module. These values are consistent with K_i values (36 μM for $NADP^+$ and 1.4 μM for 2′,5′-ADP) obtained from steady-state inhibition studies. The relatively weaker binding of $NADP^+$ to MSR compared with other members of the diflavin oxidoreductase family might arise from unique electrostatic repulsive forces near the 5′-pyrophosphate moiety and/or increased hydrophobic stacking between Trp^{697} and the *re* face of the FAD isoalloxazine ring. Small structural permutations within the NADP(H)-binding cleft have profound affects on coenzyme binding, which likely retards catalytic turnover of the enzyme in the cell. The biological implications of an attenuated mechanism of MS reactivation by MSR on methionine and folate metabolism are discussed.

Methionine synthase reductase (MSR)[1] is a key enzyme in folate and homocysteine homeostasis as it is responsible for the restoration of methionine synthase (MS) activity (*3*, *4*). MS, through two separate transmethylation reactions, liberates tetrahydrofolate from methyltetrahydrofolate and recycles homocysteine, producing methionine (Figure 1). Cobalamin serves as an intermediary in the methyl-transfer reactions and cycles between methylcobalamin and cob(I)-alamin during enzyme turnover (*5*). Occasionally (every 200−1000 catalytic turnovers) the mildly oxidizing environment of the cell converts cob(I)alamin to cob(II)alamin, rendering MS catalytically inert (*6*). Regeneration of MS activity occurs through reductive methylation of cob(II)-alamin (producing methylcobalamin), a process that couples electron transfer from MSR and methyl transfer from *S*-adenosylmethionine (*3*).

MSR (78 kDa) contains 1 equiv each of FAD and FMN. The flavins transfer electrons derived from the oxidation of NADPH to cob(II)alamin [NADPH → FAD → FMN → cob-(II)alamin (*3*, *7*)]. On the basis of the sequence and flavin topology, MSR is a member of the diflavin electron transferase family (*8*). Prokaryotic members of this family include the reductase domain of flavocytochrome P450 BM3

[†] The work was funded by the the U.K. Biotechnology and Biological Sciences Research Council (BBSRC). N.S.S. is a BBSRC Professorial Research Fellow.

[‡] Atomic coordinates and structure factors (codes 2QTZ and 2QTL) have been deposited in the Protein Data Bank, Research Collaboratory for Structural Bioinformatics, Rutgers University, New Brunswick, NJ (http://www.rcsb.org/).

* To whom correspondence should be addressed. Phone: +44 161 306 5152. Fax: +44 161 306 8918. E-mail: nigel.scrutton@manchester.ac.uk.

[1] Abbreviations: MSR, methionine synthase reductase; MS, methionine synthase; AdoMet, *S*-adenosylmethionine; AdoHcy, *S*-adenosylhomocysteine; FMN, flavin mononucleotide; FAD, flavin adenine dinucleotide; $NADP^+$ or NADP(H), nicotinamide adenine dinucleotide phosphate (reduced); NAD^+ or NAD(H), nicotinamide adenine dinucleotide (reduced); 2′,5′-ADP, 2′,5′-adenosine diphosphate; $CH_3(H_4$-folate), methyl tetrahydrofolate; H_4folate, tetrahydrofolate; NOS, nitric oxide synthase; CPR, cytochrome 450 reductase; NR1, novel reductase 1; FADD, FAD/NAD(P)H-binding module of human MSR.

10.1021/bi701209p CCC: $37.00
Published on Web 09/25/2007

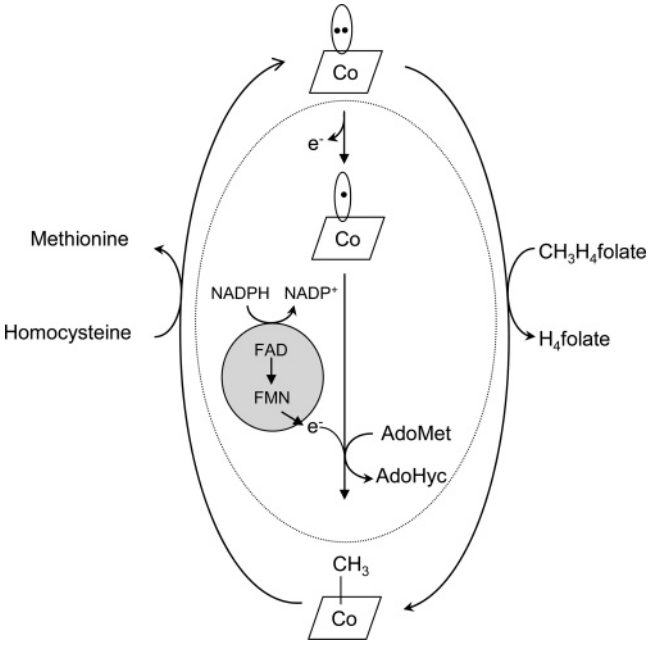

FIGURE 1: Scheme illustrating the catalytic cycle and reactivation of MS. During the primary catalytic cycle, MS uses enzyme-bound cob(I)alamin to abstract a methyl group from methyl tetrahydrofolate to generate tetrahydrofolate and methylcob(III)alamin. The methyl group is subsequently transferred to the thiol of homocysteine to produce methionine and regenerate cob(I)alamin. Every 200−1000 catalytic turnovers, cob(I)alamin oxidizes to cob(II)alamin, rendering MS catalytically inert. Reactivation of MS requires reductive methylation of cob(II)alamin, a process involving electron transfer from MSR and methyl transfer from *S*-adenosylmethionine. Reducing equivalents for the MSR-catalyzed reduction of cob(II)alamin are derived from NADPH oxidation and are delivered via the FAD and FMN redox centers of MSR.

(*9*) and the α-subunit of sulfite reductase (*10*), while eukaryotic members include cytochrome P450 reductase (*11*, *12*), the nitric oxide synthases (NOSs; *13*, *14*), and novel oxidoreductase 1 (NR1; *15*). Diagnostic features for this family of enzymes include (i) an FMN cofactor housed in a domain homologous to bacterial flavodoxin (*16*), (ii) adjacent NADP(H)- and FAD-binding domains that are structurally related to ferredoxin-NADP(H) reductase (FNR; *17*), (iii) a connecting domain that bridges the flavin domains, and (iv) a "linker" or hinge that tethers the FMN domain with the connecting domain. In crystal structures of CPR (*12*) and neuronal NOS (*18*), the hinge region (14−24 residues in length) located between the flavin-binding domains is partially disordered, pointing to a dynamic role. For nNOS, it has been suggested that the hinge allows the FMN domain to swing between the FAD domain and the heme oxygenase domain, to enable electron transfer between the two redox centers (*18*, *19*). In MSR, the region of protein separating the connecting domain and the FMN domain is extensively longer (82 residues), leading us to speculate that this section of the polypeptide might allow the FMN domain to shuttle electrons between the FNR-like module of MSR and cob(II)alamin during the regeneration of MS in a mechanism that involves large-scale motion of the FMN domain (*2*).

Alignment of primary sequences for members of the diflavin reductase family suggests a lack of sequence conservation in the NADP(H)-binding site of MSR (Figure 2). In particular, variation exists within the sequence of highly conserved residues that form hydrogen bonds and electrostatic contacts with the 2′-phosphoryl group of NADPH. The crystal structure of spinach FNR showed that the 2′-phosphate of NADP(H) is anchored through a network of electrostatic interactions by residues Ser^{234}, Arg^{235}, Tyr^{246}, and Lys^{244} (*17*, *20*). Lys^{244} is more remote than the other residues from the 2′-phosphate in the FNR structure and therefore constitutes a weaker interaction with the phosphate. These core residues enable the enzyme to discriminate between NADPH and NADH (*21*). Early chemical modification and mutagenesis experiments established that the corresponding residues in CPR, in particular Arg^{597} and Lys^{602}, are also important for binding of NADP(H) (*22*). Arg^{597} was shown to contribute significantly to the binding energy (5 kcal/mol) and to be a key determinant for discriminating between NADPH and NADH (*23*). Subsequent crystal structures of CPR (*12*) and nNOS (*18*, *24*) have established that these two residues, along with Ser^{596} and Tyr^{604} (CPR numbering), form a consensus sequence for binding the 2′-phosphate group of NADP(H). Sequence alignment suggests that MSR does not rigorously adhere to this consensus sequence motif for binding the 2′-phosphate as it possesses only three of the four binding determinants, Ser^{610}, Arg^{611}, and Tyr^{624} (MSR numbering), in the correct positions. A lysine residue, another candidate for neutralization of 2′-phosphate, is at position 623 in MSR rather than the expected position of 622. Also, a six amino acid insert extends the distance between neighboring Ser^{610}/Arg^{611} and Tyr^{624} (MSR numbering, Figure 2). This apparent structural variation within the coenzyme-binding site of MSR might account (at least in part) for why previous rapid kinetic studies have pointed to an elevated dissociation constant for the NADP(H)−MSR complex relative to other members of the family (*7*).

In this paper, we report the crystal structure of the MSR FAD/NADP(H)-binding module complexed with $NADP^+$. In light of the sequence divergence in the 2′-phosphate-binding site, we examined the substrate specificity of MSR for NADPH and NADH. We have used isothermal titration calorimetry in conjunction with inhibition studies to investigate the binding properties of the coenzyme and the competitive inhibitor 2′,5′-ADP, and we rationalize these findings in the context of the structure of the FAD/NAD(P)H-binding module−$NADP^+$ complex and biological function. The structure of the FAD/NADP(H)-binding module−$NADP^+$ complex has allowed us to examine, at the molecular level, the potential impact of clinically relevant mutants of MSR, which are known to impair enzyme function and contribute to hyperhomocysteinemia and megaloblastic anemia (*4*, *25*).

EXPERIMENTAL PROCEDURES

Purification, Crystallogenesis, and Data Collection. Recombinant human MSR and the NADP(H)/FAD domain (residues 163−698) were expressed and purified according to published procedures (*26*). Crystals of the MSR NADP(H)/FAD domain were grown using the sitting drop vapor diffusion method at 4 °C. The enzyme (10 mg/mL) was desalted into 10 mM Tris/HCl, pH 8.0, containing 0.5 mM DTT, 1 mM EDTA, and 0.05% NaN_3. Crystals were obtained with four different precipitant conditions, but crystals that diffracted to higher resolution were obtained with the reservoir solution comprising 0.1 M Tris/HCl, pH 7.5, 0.2

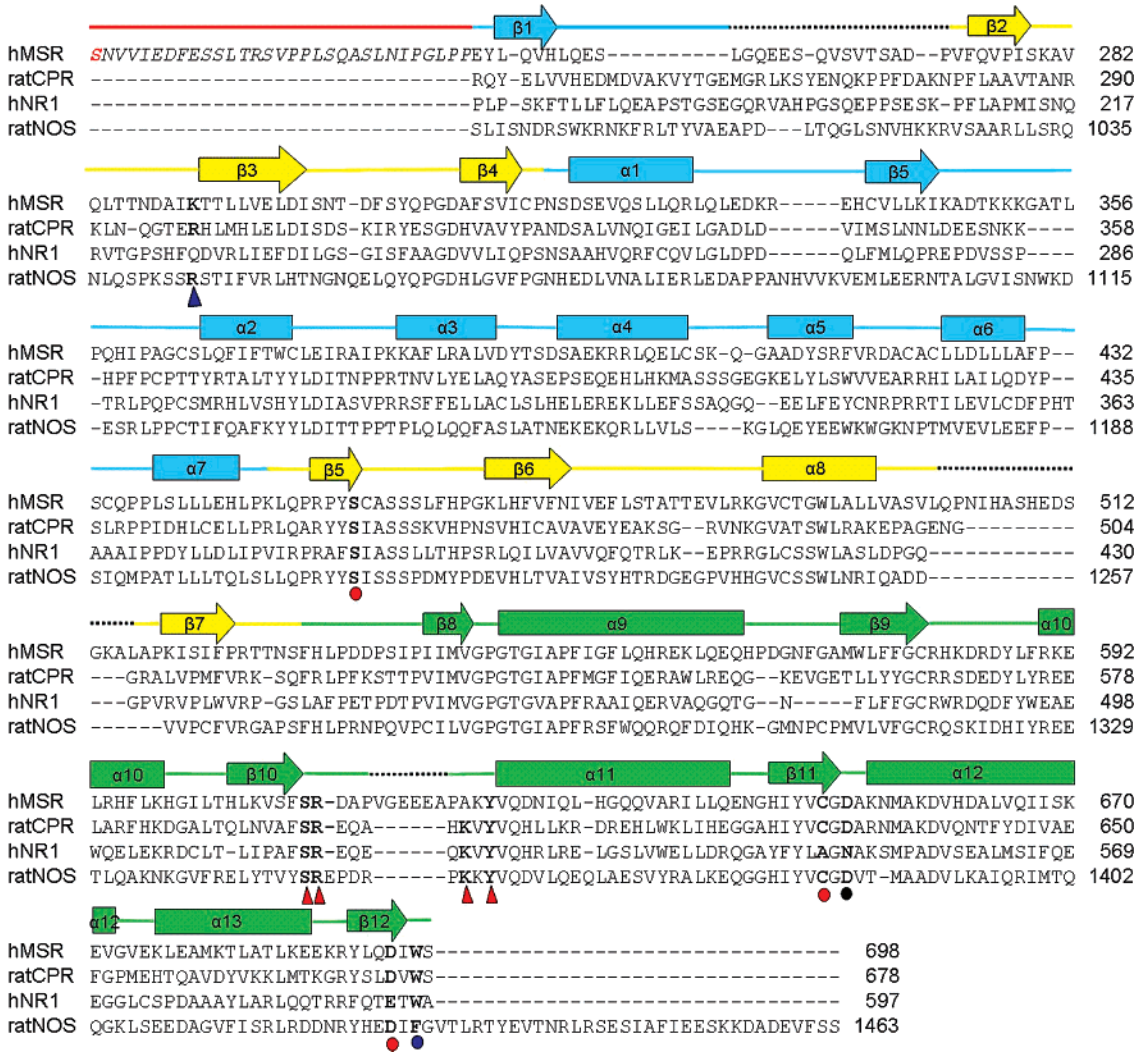

FIGURE 2: Structure-based sequence alignment of the human MSR (hMSR) FAD/NADP(H)-binding module against the corresponding sequences of rat CPR, rat neuronal NOS (ratNOS), and human NR1 (hNR1). Secondary structural elements are shown above the sequence. β-strands are shown as arrows, and α-helices are indicated by rectangles. Nonvisible regions are indicated by dashed lines, and residues belonging to the hinge, connecting domain, FAD domain, and NADPH-binding domain are colored red, blue, yellow, and green, respectively. The residue colored red is the first ordered residue in the structure. Key residues, denoted by symbols below the sequence, are as follows: the blue triangle is for the residue which forms a hydrogen bond to the 5′-phosphate of $NADP^+$, red circles denote residues which form part of the catalytic triad for hydride transfer, red triangles are for residues which stabilize the 2′-phosphate of $NADP^+$, the black circle indicates the aspartic acid residue which is solvent exposed and lies between the 5′-pyrophosphate of $NADP^+$ and the isoalloxazine ring of FAD, and the blue circle is for the aromatic residue which lies over the *re* face of the isoalloxazine ring of FAD in the crystal structure.

M KBr, and 15% PEG 4000. The crystals were soaked in a 50:50 mix of Paratone and mineral oil (cryoprotectant) before being flash-cooled in liquid nitrogen. A few crystals were soaked in mother liquor supplemented with a saturating level of $NADP^+$ before cryoprotection. Data sets at 1.9 Å resolution were collected for the MSR NADP(H)/FAD module with and without $NADP^+$ bound at the European Synchrotron Radiation Facility (Grenoble, France) on ID14-EH3 using an ADSC Q4 CCD detector.

Structure Determination and Refinement. Data were processed and scaled using the HKL package programs DENZO and SCALEPACK (*27*). The structure was solved via molecular replacement using the program AMoRE (*28*) and the NADP(H)/FAD module of the deposited structure of cytochrome P450 reductase (CPR; *12*) as the search model (PDB code 1AMO). Positional and *B*-factor refinement was performed using REFMAC5, using both restrained (*29*) and TLS (*30*) modes, with alternate rounds of manual rebuilding of the model in TURBO-FRODO (*31*) and COOT (*32*). Partial rebuilding of the model and building of waters were carried out using ARP/wARP (*33*). The quality of the model was checked using the program Molprobity (*34*).

Isothermal Titration Calorimetry (ITC). ITC experiments were performed using a VP-ITC microcalorimeter (Microcal Inc.). Protein samples were dialyzed into 50 mM Tris/HCl, pH 7.5. The concentrations of MSR and the FAD/NAD(P)H-binding module were determined by the absorbance value at 454 nm using extinction coefficients of 25 600 and 11 200 M^{-1} cm^{-1}, respectively (*26*). Experiments were performed at 25 °C, and protein solutions were degassed by vacuum aspiration for 8 min at 23 °C prior to loading of the samples into the ITC cell and syringe. Aliquots (10 μL) of the nucleotide were titrated into 1.28 mL of 40−100 μM MSR or the isolated FAD/NAD(P)H-binding module at 420 s intervals with a stirring speed of 350 rpm. Parallel experiments were performed by injecting the nucleotide into the buffer. The heats of dilution were negligible and subtracted from their respective titrations prior to data analysis.

Thermodynamic parameters n (stoichiometry), K_d ($1/K_a$, the association constant), and $\Delta^\circ H$ (enthalpy change) were obtained by nonlinear least-squares fitting of experimental data using the single-site binding model of the Origin software package (version 7.0) provided with the instrument. The free energy of binding (ΔG°) and entropy change (ΔS°) were obtained using eqs 1 and 2.

$$\Delta G^\circ = -RT \ln K_A \quad (1)$$

$$\Delta G^\circ = \Delta H^\circ - T\Delta S^\circ \quad (2)$$

Steady-State Turnover Assays. Kinetic assays were performed in a 1.0 mL volume at 25 °C using a 1 cm path length cuvette by measuring the absorbance change at 550 nm associated with the reduction of cytochrome c^{3+} ($\Delta\epsilon$ = 21 100 M^{-1} cm^{-1}; *35*). The reaction mixtures contained 50 mM Tris/HCl, pH 7.5, 8 μM cytochrome c^{3+}, and variable concentrations of NADPH and NADH. For inhibition assays, the reaction mixtures contained 50 mM Tris/HCl, pH 7.5, 8 μM cytochrome c[3], and variable concentrations of the substrate, NADPH, and inhibitor ($NADP^+$, 2′,5′-ADP). Reactions containing NADPH and NADH were initiated by the addition of 12.2×10^{-12} and 122×10^{-12} mol of MSR, respectively. Data from the substrate specificity studies were fit to the Michaelis−Menten equation, while data for the inhibition studies were fit with nonlinear least-squares analysis to the equation for competitive inhibition (eq 3)

$$v_i = \frac{VA}{K_m(1 + I/K_i) + A} \quad (3)$$

using the computer program Origin, version 7.0 (MicroCal Software Inc.), where v_i is the initial velocity, V is the maximal velocity, A is the varied substrate concentration, K_m is the apparent Michaelis constant, I is the inhibitor concentration, and K_i is the inhibition constant.

RESULTS

Overall Domain Architecture. The structure of the FAD/NADP(H)-binding module of MSR was solved by molecular replacement using a truncated structure of CPR as the initial model (*12*). The crystallographic and final refinement statistics are summarized in Table 1. The structure consists of 448 visible residues starting from residue Ser^{217} and ending at Ser^{698} (Figure 2). The first 54 residues are disordered, as are flexible regions Leu^{258}−Asp^{271}, Gln^{502}−Ala^{515}, and Val^{615}−Ala^{620}. From the N- to C- terminus, the truncated protein comprises the hinge, the connecting domain, the FAD domain, and the NADPH-binding domain. The NADP(H)-binding domain comprises an $\alpha\beta\alpha$ structural motif (five-stranded parallel β-sheet sandwiched between six α-helices), and the core of the FAD-binding domain is a flattened antiparallel β-barrel, comprising six β-strands (Figure 3). Both domains are similar to the corresponding domains of NOS (*18*), CPR (*12*), and FNR (*17*) and the NAD^+ domains of cytochrome b_5 reductase (*36*) and phthalate dioxygenase reductase (*37*). The connecting domain, which consists principally of α-helices, is structurally integrated with the FAD domain. Three β-strands of the FAD-binding domain are inserted into the connecting domain (Figure 2). The connecting domain is unique among the diflavin reductase family (CPR, NOS, NR1, bacterial P450 BM3, and the α-subunit of sulfite reductase) and is believed to be responsible for dictating the relative orientation of the FAD- and FMN-binding domains.

Table 1: Crystallographic Data and Refinement Values for the FAD/NAD(P)H-Binding Module of Human MSR with and without $NADP^+$ Bound[a]

	$NADP^+$-free structure	$NADP^+$-bound structure
	Data Collection	
resolution limits (Å)	20−1.9 (1.95−1.90)	20−1.9 (1.95−1.90)
space group	$P2_1$	$P2_1$
unit cell (Å)	a = 52.6, b = 67.3, c = 78.8	a = 51.8, b = 67.2, c = 78.6
β angle (deg)	107.7	107.0
total no. of reflns	593 861	644 500
no. of unique reflns	39 892	39 791
redundancy	3.5	3.6
completeness (%)	100.0 (100.0)	100.0 (100.0)
$I/\sigma(I)$	25.3 (3.1)	23.6 (3.3)
R_{merge} (%)	4.0 (26.1)	5.2 (30.4)
solvent content (%)	45	44
	Refinement	
no. of residues	448	447
no. of water molecules	498	359
R_{fac}/R_{free} (%)	18.4/23.2 (22.9/35.8)	17.6/21.2 (19.7/26.5)
RMSD(bond lengths) (Å)	0.016	0.014
RMSD(bond angles) (deg)	1.527	1.493
av B-factor (Å^2)	31.2	29.3
	Ramachandran plot	
most favored regions (%)	98.9	99.1
additionally allowed regions (%)	0.9	0.7
outliers	0.2 (Gly^{544})	0.2 (Gly^{544})

[a] Numbers in parentheses represent the last outer shell (1.95−1.90 Å).

Extended Hinge Region. A distinguishing feature that emerges from structure-based sequence alignment between MSR and related diflavin reductases is an 82 amino acid insert (Ala^{166} to Pro^{247}) between the FMN domain and the connecting domain of MSR. Although the insertion lies at the boundary of the flexible "hinge" region and the connecting domain, we have assigned these residues to the former, on the basis of superposition of the MSR structure with that of rat CPR (*12*). The last (i.e., C-terminal) 31 residues of the extended hinge are visible in the truncated MSR structure (Ser^{217}−Pro^{247}) (Figure 3). The position of the initial seven visible residues (Ser^{217} to Asp^{223}) is thought to be nonphysiological as these residues interact with a symmetry-related molecule (Figure S1 of the Supporting Information). This is likely to be a consequence of the truncation of the protein and/or crystal packing. Residues Ser^{227} to Pro^{247} form a random coil at the surface of the connecting domain, which wraps partially around the axis of three short α-helices (Figure S2 of the Supporting Information). Again, as this is a structure of a truncated protein, it is uncertain as to whether the position of these residues is physiologically relevant or a consequence of crystal packing. However, an analysis of the interface between the extended hinge and other parts of the connecting domain shows that up to 41 hydrogen bond contacts and salt bridges are formed, excluding water contacts. A shape complementarity (S_c) value of 0.781 over this protein

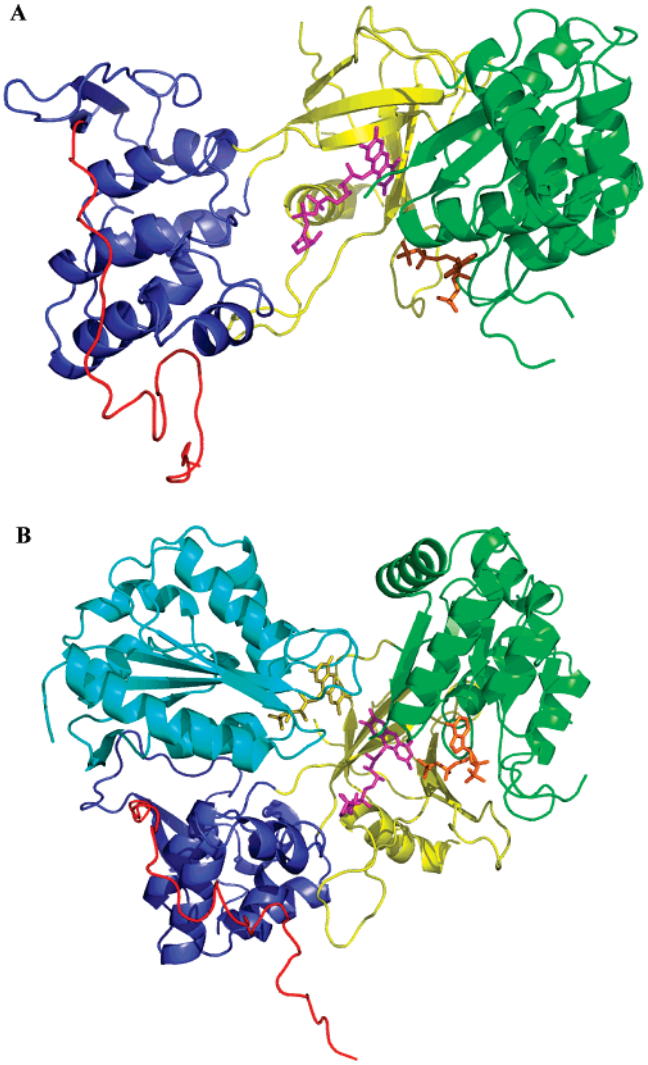

FIGURE 3: A cartoon representation of the human MSR FAD/NADP(H)-binding module. The extended hinge region is in red, and the connecting domain, FAD domain, and NADPH-binding domain are in blue, yellow, and green, respectively. The FAD (magenta) and the $NADP^+$ (orange) of MSR are shown in stick format. (B) Structure of the human MSR FAD/NADP(H)-binding module superimposed with that for CPR (PBD 1AMO), with only the FMN domain (cyan) and the FMN cofactor (yellow stick format) of CPR showing. The MSR FAD/NADP(H)-binding module is shown as in panel A.

interface is within the range expected for biologically relevant protein−protein interactions, lending further support for the structure representing a physiologically relevant conformation (*38*). The binding of the coenzyme does not affect the position of the hinge as it is in the same position in the $NADP^+$-free structure.

On the basis of the structures of the reductase domain of nNOS and CPR, it is anticipated that the remainder of the extended hinge (which is absent from the MSR FAD/NADP(H) domain structure) folds behind the connecting domain, to position the FMN domain at the binding interface between the FAD- and NADPH-binding domains (Figure 3). The location of the FMN domain observed in CPR and nNOS accommodates direct interflavin electron transfer as the isoalloxazine rings of FAD and FMN are separated by ~4−5 Å. The lack of electron density for the first 54 residues of the protein structure highlights the flexibility of the extended region in MSR and the possibility of it enabling the FMN-binding domain to "toggle" between MS and the MSR FNR module during electron transfer.

FAD Binding Site. In the MSR FAD/NADP(H)-binding module, the FAD cofactor is bound in an extended conformation. The isoalloxazine ring of the FAD molecule is bound at the interface between the FAD- and NADPH-binding domains and is stabilized by hydrophobic interactions and several hydrogen bond contacts with the protein (Figure 4). The O2 atom of the isoalloxazine ring forms hydrogen bonds with the main chain atoms of Ser^{454} (amide nitrogen) and a water molecule. The N3 atom makes hydrogen bond contacts with Val^{469} (carbonyl oxygen), and the N5 and O4 atoms of the ring form hydrogen bonds with individual water molecules. The negative charges on the pyrophosphate group are neutralized by water molecules, as well as the amide nitrogen and hydroxyl group of Thr^{490}, the side chain of Arg^{451}, and the peptide backbone of residues Cys^{489} and Val^{488}. In the MSR structure, the electron density for the ribose shows that it can occupy more than one position in the structure (Figure S3 of the Supporting Information). The electron density shows that residue Cys^{421}, located near the ribose sugar, is partially oxidized to cysteinic acid, which could account in part for the multiple positions observed for this portion of the FAD molecule. We have modeled the ribose into one of its positions, as in the second position the OD atom of the oxidized cysteine clashes with the AC1 atom of the ribose. The orientation of the sugar in MSR is quite different from the modeled position in CPR (Figure 4B; *12*). The dynamic nature of the ribose may in turn increase the mobility of the adenine ring for which there is no electron density.

Superposition of the FAD-binding site of the MSR NADP(H)/FAD module with that of CPR also reveals that conserved residues which form a catalytic triad for hydride transfer in CPR (Cys^{630}, Asp^{675}, and Ser^{457}) are in the same position in MSR (Figure 4C; *39*, *40*), suggesting that the mechanism of hydride transfer from NADPH to FAD is similar in both enzymes.

$NADP^+$-Binding Site. $NADP^+$ binds at one end of a β sheet. As in CPR (*12*) and FNR (*17*), the solvent-exposed ribitylnicotinamide ring of the coenzyme is disordered in the structure and only the 2′-phosphoryl-AMP moiety of the molecule is observed. In nNOS, the entire $NADP^+$ molecule is observed but it is not found in a conformation compatible with hydride transfer as the ribose−nicotinamide moiety is located at the surface of the protein and does not have any strong interactions with the polypeptide (*18*, *24*).

Despite sequence divergence in the 2′-phosphate-binding motif, the overall binding geometry of the 2′-phosphate of $NADP^+$ in MSR is similar to that observed in CPR and other related flavoenzymes (*12*, *18*, *40*, *41*). A superposition of the nicotinamide-binding sites for MSR and CPR (Figure 5) illustrates that, in the MSR structure, the lysine residue, which is displaced in the consensus sequence, is replaced by a water molecule, which forms a hydrogen bond with an oxygen atom (AOP2) of the 2′-phosphate. In CPR, the hydroxyl groups of Ser^{596} and Tyr^{604} and NZ and NE atoms of Arg^{597} and Lys^{602} (respectively) interact with the 2′-phosphate of $NADP^+$ (*12*). In MSR, three of the four residues (Ser^{610}, Arg^{611}, and Tyr^{624}) of the binding motif also stabilize the 2′-phosphate. In addition, three well-ordered water molecules form hydrogen bonds with the 2′-phosphate in

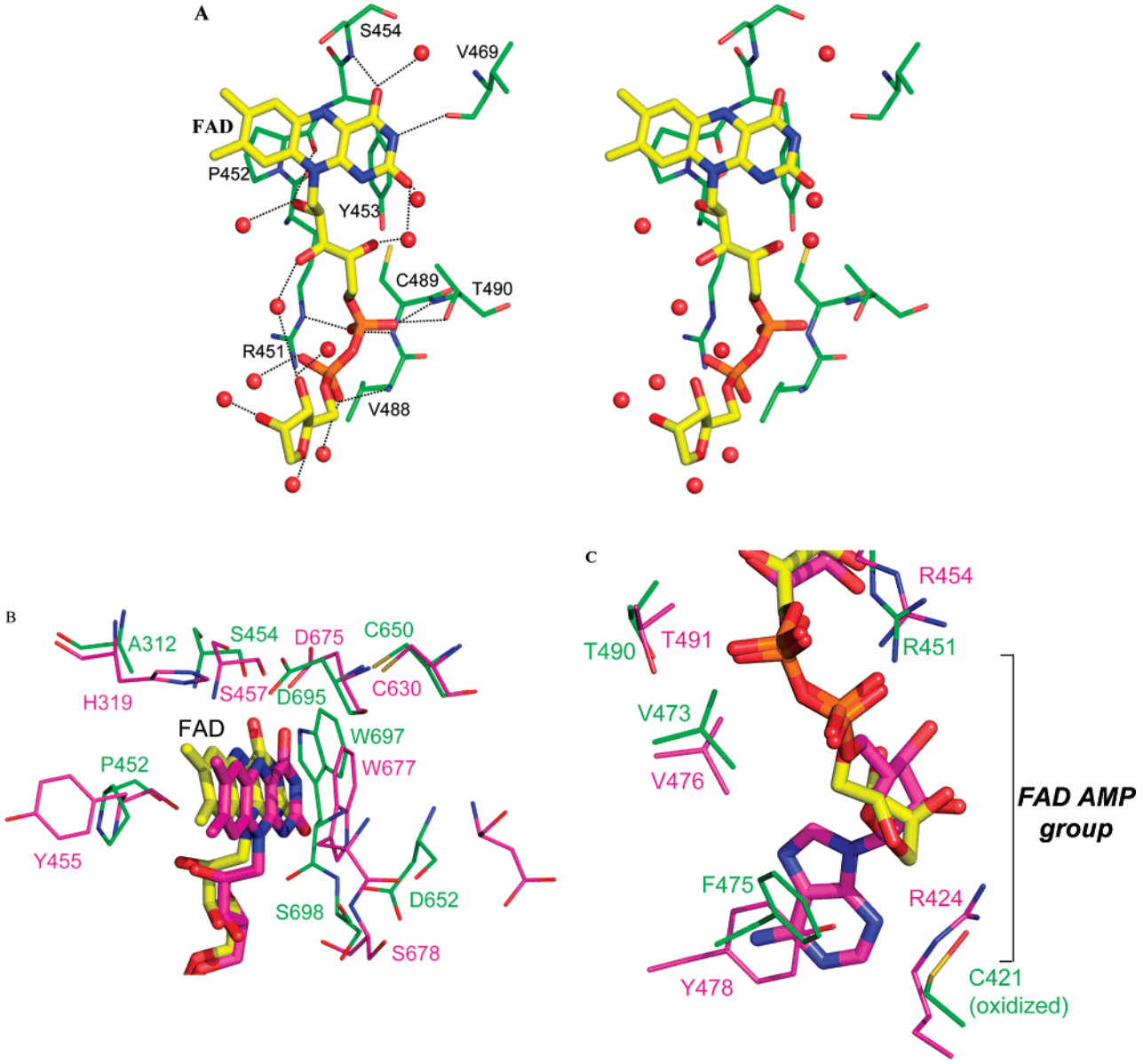

FIGURE 4: (A) Stereodiagram of the FAD binding in MSR. FAD and residues are shown as atom-colored sticks and lines, respectively. Water molecules are denoted by red spheres. Interactions are shown as dotted lines. (B) Superposition of the MSR and rat CPR FAD isoalloxazine-binding sites. FAD and residues are shown as atom-colored sticks and lines, respectively. MSR and CPR carbons are shown as green and magenta atoms, respectively. (C) Superposition of the MSR and rat CPR FAD AMP-binding sites. FAD and residues are shown as atom-colored sticks and lines, respectively. MSR and CPR carbons are shown as green and magenta, respectively. The structure of CPR is from the following PDB entry: 1AMO.

MSR. Although Lys^{623} is localized near the binding site, the residue is solvent exposed and does not form any electrostatic or hydrogen bond contacts with the coenzyme. The six amino acid insert in the MSR consensus sequence for the 2′-phosphate binding is disordered in the structure. This stretch of amino acids likely represents a mobile loop, and it is unclear how or whether this region affects nicotinamide binding or influences the catalytic behavior of the enzyme.

Substrate Specificity. The network of residues stabilizing the 2′-phosphate of the nicotinamide enables the enzyme to discriminate between NADH and NADPH. The divergence in the consensus sequence for MSR (Figure 2) suggests that the preference of the enzyme for NADPH over NADH may be different from that observed for other members of the FNR extended family. To determine the substrate specificity, the rate of MSR-catalyzed reduction of cytochrome c^{3+}, a nonphysiological electron acceptor, was measured in the presence of increasing concentrations of NADH or NADPH. The steady-state kinetic parameters for both coenzymes are summarized in Table 2. The specificity for NADPH versus NADH is 19 400, similar to the value reported for CPR (23 250; *42*) and slightly greater than the values reported for nNOS (4987; *43*) and P450 BM3 (8571; *44*). Spinach FNR has the greatest specificity for NADPH over NADH, as the ratio for this enzyme is 67 500 (*45*). As the relative preference of MSR for NADPH over NADH is within the range expected for this family of enzymes, the absence of a conserved lysine residue and insertion of six amino acids in the consensus sequence do not markedly influence the coenzyme specificity of MSR.

Isothermal Titration Calorimetry. ITC was used to investigate whether the structural difference observed in the $NADP^+$-binding site between MSR and CPR affects the binding affinity for the nicotinamide coenzyme. The ther-

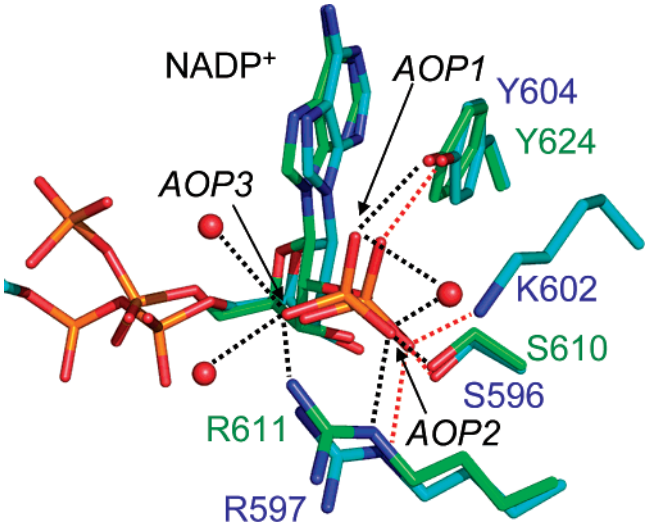

FIGURE 5: Superposition of the MSR and rat CPR 2′-phosphate-binding sites. The color scheme is as follows: oxygen, red; nitrogen, blue; carbon of CPR, cyan; carbon of MSR, green; phosphorus, orange. Residue numbers for MSR are written in green, and those for CPR are in blue. Individual oxygen atoms of the 2′-phosphate are labeled in italics. Hydrogen bond contacts in MSR and CPR are denoted by black and red dashed lines, respectively, and water molecules are red spheres. The structure of CPR is from the following PDB file: 1JA1.

Table 2: Kinetic Constants for MSR-Catalyzed Reduction of Cytochrome c^{3+} with NADH and NADPH

substrate	k_{cat} (s^{-1})	K_m ($M \times 10^{-6}$)	k_{cat}/K_m ($s^{-1}\ M^{-1} \times 10^{-3}$)	(k_{cat}/K_{NADPH})/(k_{cat}/K_{NADH})
NADH	0.24 ± 0.03	3540 ± 560	0.0678 ± 0.0137	
NADPH	3.92 ± 0.10	2.89 ± 0.18	1315.4 ± 88.5	19 400

modynamic binding parameters were also determined for the competitive inhibitor 2′,5′-ADP to isolate the contribution in binding energy from the phosphoryladenosyl portion of the molecule. Figure 6 represents the ITC binding isotherms resulting from the titration of the isolated FAD/NADP(H)-binding module or full-length MSR with $NADP^+$ or 2′,5′-ADP. In all cases, the binding isotherms were exothermic and fit to a single-site model. The calculated binding stoichiometry is ~1 for all four titrations (Table 3). The observed dissociation constant (K_d) for the protein−$NADP^+$ complexes with the FAD/NADP(H)-binding module (Figure 6A) or full-length MSR (Figure 6C) is ~36 μM (Table 3). The competitive inhibitor 2′,5′-ADP exhibits tighter binding to the NADP(H)/FAD-binding module (Figure 6B) and the full-length enzyme (Figure 6D) as the dissociation constant is ~1−2 μM. Similar values for the dissociation constant have been reported for interaction of 2′,5′-ADP nNOS (*19*) and FNR (*46*). However, the binding of 2′,5′-ADP to CPR is substantially tighter (K_d = 53 nM; *47*). Tighter binding of 2′,5′-ADP to CPR might be due to more stable interaction with the 2′-phosphate and/or the pyrophosphate moiety. More significantly, the dissociation constant for $NADP^+$−MSR (37 μM) is close to ~700-fold weaker than that for the $NADP^+$−CPR complex (K_d = 53 nM; *47*). With CPR, the dissociation constants for the $NADP^+$ and 2′,5′-ADP complexes have essentially identical values, indicating that the binding energy for the coenzyme is supplied almost entirely through the 2′,5′-ADP moiety and that the ribitylnicotinamide group does not contribute significantly to stabilizing the protein−coenzyme

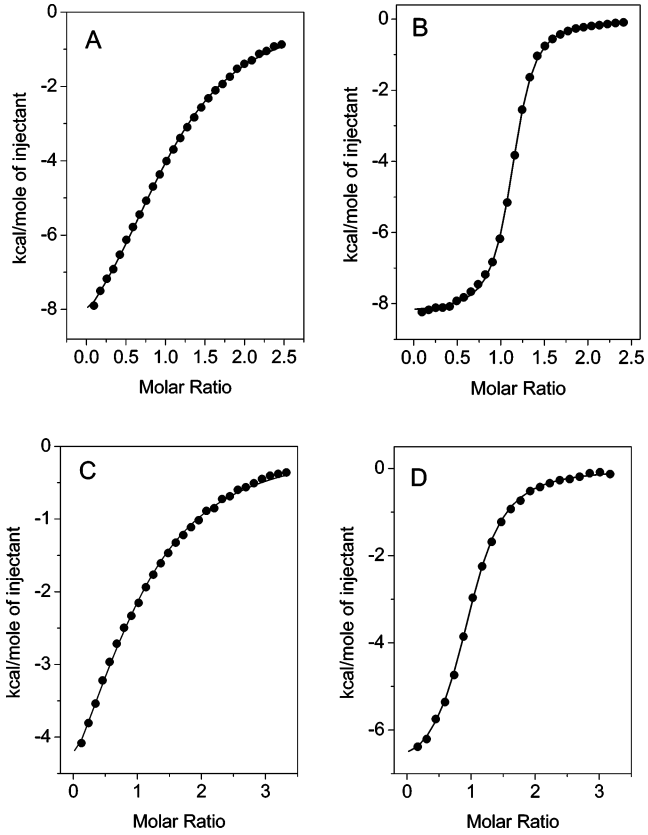

FIGURE 6: Binding isotherms for the titration of MSR and the isolated NADP(H)/FAD domain with $NADP^+$ and 2′,5′-ADP: (A) titration of $NADP^+$ into the FAD domain, (B) titration of 2′,5′-ADP into the FAD domain, (C) titration of $NADP^+$ into MSR, and (D) titration of 2′,5′-ADP into MSR. The MSR and FAD domain concentrations were between 40 and 90 μM, while the $NADP^+$ and 2′,5′-ADP concentrations were between 1.0 and 1.5 mM. All titrations were performed in 50 mM Tris/HCl, pH 7.5, at 25 °C, and the data in all four titrations were fit to a one-site model as described in the Experimental Procedures. The thermodynamic binding parameters $\Delta S°$, $\Delta G°$, $\Delta H°$, and K_d for the binding isotherms are listed in Table 3.

complex. By contrast, the ribitylnicotinamide portion of $NADP^+$ reduces the binding of the coenzyme in MSR, as the dissociation constant for $NADP^+$ is nearly 30-fold weaker than that for 2′,5′-ADP.

Steady-State Inhibition of Cytochrome c^{3+} Reduction. $NADP^+$ and 2′,5′-ADP were used as inhibitors of MSR-catalyzed reduction of cytochrome c^{3+} to determine whether the observed difference in dissociation constants (K_d) for complexes formed with $NADP^+$ and 2′,5′-ADP were manifest as variations in the steady-state inhibition constants (K_i). Double-reciprocal plots of initial velocity versus NADPH concentration at several fixed concentrations of $NADP^+$ or 2′,5′-ADP indicated that both substrates are competitive versus NADPH. The inhibition data fitted to eq 3 (Table 4) revealed that 2′,5′-ADP (K_i = 2 μM) is a stronger inhibitor for NADPH-catalyzed reduction of cytochrome c^{3+} than $NADP^+$ (K_i = 37 μM). For both inhibitors, the apparent inhibition constants are essentially the same as the dissociation constants determined by ITC. The apparent dissociation constants for NADPH and $NADP^+$ determined from single-turnover stopped-flow studies ranged between 37 and 60 μM (*7*).

Comparison of Electrostatic Surfaces in the NADP(H)-Binding Cleft. In an attempt to interpret the substantial

Table 3: Thermodynamic Parameters for Binding of $NADP^+$ and 2′,5′-ADP to MSR and the FAD/NADP(H)-Binding Module of MSR As Determined by Isothermal Titration Calorimetry

	ligand	K_d (μM)	n	$\Delta H°$ (kJ/mol)	$\Delta G°$ (kJ/mol)	$\Delta S°$ (cal mol^{-1} K^{-1})
MSR	$NADP^+$	34.5 ± 1.7	0.98 ± 0.01	−29.98 ± 0.95	−25.47 ± 1.16	−11.81 ± 1.65
FADD[a]	$NADP^+$	35.1 ± 0.4	1.11 ± 0.01	−40.12 ± 0.50	−25.06 ± 0.33	−50.36 ± 2.06
MSR	2′,5′-ADP	2.4 ± 0.1	0.96 ± 0.01	−29.39 ± 0.21	−32.03 ± 0.08	−7.43 ± 0.83
FADD	2′,5′-ADP	1.4 ± 0.1	1.11 ± 0.01	−34.10 ± 0.21	−32.94 ± 0.21	−3.88 ± 0.74
CPR[b]	$NADP^+$	0.053	1.0	−70.2	−39.62	
CPR[b]	2′,5′-ADP	0.050	1.1	−74.3	−40.45	

[a] FADD is defined as the FAD/NAD(P)H-binding module of human MSR. [b] The values are from ref *47*.

Table 4: Kinetic and Inhibition Constants for MSR-Catalyzed Reduction of Cytochrome c^{3+} with NADPH[a]

inhibitor	k_{cat} (s^{-1})	K_{NADPH} (μM)	K_i (μM)
$NADP^+$	7.23 ± 0.14	2.37 ± 0.17	36.89 ± 2.70
2′,5′-ADP	6.62 ± 0.13	1.95 ± 0.14	1.44 ± 0.11

[a] The values for K_i were determined as described in the Experimental Procedures.

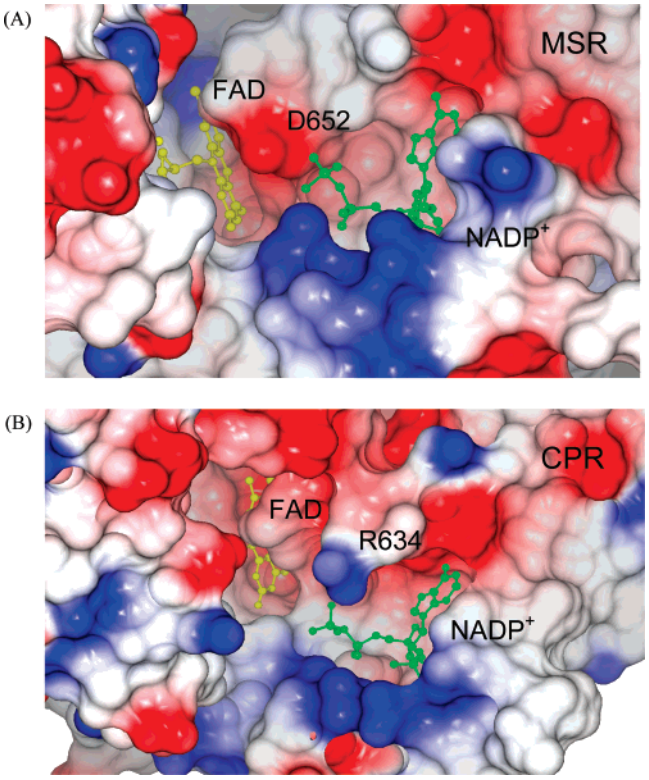

FIGURE 7: Comparison of the electrostatic surfaces of the $NADP^+$-binding pockets in MSR (A) and CPR (B). $NADP^+$ and FAD are shown as green and yellow balls and sticks, respectively, and the Asp^{652} of MSR and Arg^{634} of CPR are labeled. The electrostatic surface is shown as blue for a positive potential and red for a negative potential. The structure of CPR is from the following PDB entry: 1AMO. The orientation was shifted between panels A and B to observe the FAD and $NADP^+$ molecules in CPR and MSR.

differences in affinities for $NADP^+$ and 2′,5′-ADP for MSR and CPR, electrostatic surfaces for the nicotinamide-binding sites of both enzymes were generated (Figure 7). The volume of the $NADP^+$/FAD-binding cavity, calculated using the program CASTp (*48*), is significantly smaller in MSR (1408 $Å^3$) compared to CPR (1768 $Å^3$). The differences in charge around the FAD isoalloxazine ring likely account for differences in redox potential values for the FAD cofactor between the two enzymes (*26*, *49*). While the binding pocket around the 2′-phosphate is positively charged for both enzymes, the binding cavity around the 5′-pyrophosphate group is more negatively charged in MSR compared to CPR. In particular, the solvent-exposed residue Asp^{652} of MSR is positioned between the 5′-pyrophosphate and the isoalloxazine ring of FAD (Figure 7A). The carboxylate side chain of Asp^{652} has a large *B*-factor value, suggesting a degree of mobility for this side chain. In comparison, the carboxylate side chain of the corresponding residue in CPR (Asp^{632}) is in a different position, pointing away from the isoalloxazine ring (Figure 8A). The pyrophosphate group of $NADP^+$ in the CPR structure is stabilized by the amide nitrogen of Thr^{535} and through weak hydrogen bonds with the side chain of Arg^{298}. The pyrophosphate group in the MSR−$NADP^+$ complex is stabilized through weak interactions with the side chain of Lys^{291}, the side chain of Ala^{653}, and two water molecules. These notable differences in residues surrounding the pyrophosphate group in the MSR−$NADP^+$ and CPR−$NADP^+$ complexes likely shift the orientation of the pyrophosphate group to a more solvent-exposed position in the MSR−$NADP^+$ complex.

In MSR, destabilization of $NADP^+$ binding by the ribitylnicotinamide ring might arise from the unique position of the indole ring of Trp^{697} over the *re* face of the FAD isoalloxazine ring. For hydride transfer, the nicotinamide ring must stack against the same face of the isoalloxazine ring so that the C4 atom of NADPH is in close proximity to the N5 atom of FAD. To facilitate this, Trp^{697} must swing away from the FAD to avoid steric clashes with the nicotinamide ring. The movement of this tryptophan residue has been observed in stopped-flow fluorescence studies, and the rate constant for this process is similar to the rate constant for hydride transfer (*7*). An overlay of the FAD isoalloxazine rings and the conserved tryptophan residues for MSR and CPR reveals a different orientation for the aromatic stacking residue (Figure 4B). In MSR, the entire indole ring of the tryptophan residue stacks against the isoalloxazine ring, whereas in CPR the tryptophan side chain (Trp^{677}) is oriented approximately 90° with respect to this residue in MSR so that only the benzyl moiety of this residue stacks against the isoalloxazine ring. Additional $\pi-\pi$ interactions between the isoalloxazine ring and the MSR Trp^{697} indole ring likely result in greater thermodynamic stability for this conformational state and possibly weaker binding of the coenzyme. The crystal structure of the NADP(H)/FAD module without $NADP^+$ bound reveals that binding of the coenzyme does not alter the orientation or position of residues Trp^{697} and Asp^{652}.

However, it is likely that Asp^{652} of MSR moves for hydride transfer to occur, as a superposition of the MSR structure with that of a W677G mutant form of CPR shows that there would be a steric clash between the ribose of $NADP^+$ and

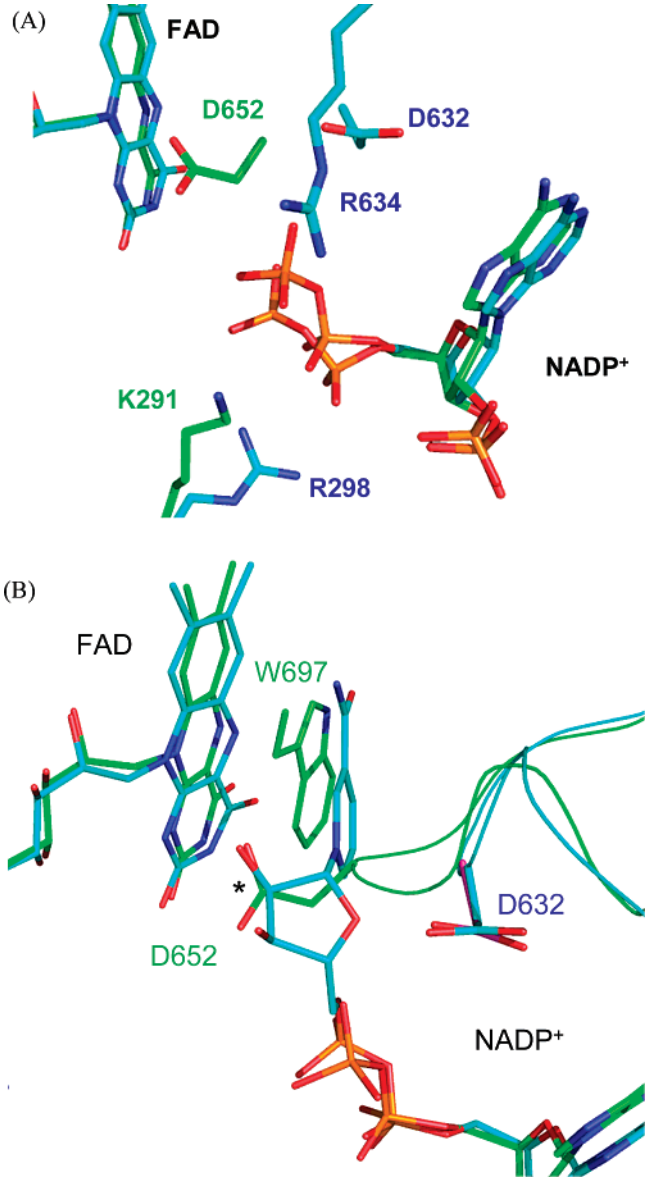

FIGURE 8: (A) Superposition of the pyrophosphate-binding site for $NADP^+$ in MSR and CPR (PDB entry 1AMO). In MSR, Asp^{652} of MSR is positioned between the pyrophosphate group and the isoalloxazine ring of FAD, whereas the corresponding residue in CPR, Asp^{632}, is removed from the vicinity of the pyrophosphate group. (B) Superposition of the pyrophosphate-binding site for $NADP^+$ in MSR with wild-type CPR (PDB entry 1AMO) and a W677G mutant of CPR (PDB entry 1J9Z). The W677G mutant structure of CPR shows the nicotinamide ring of $NADP^+$ stacked against the FAD isoalloxazine ring. The asterisk denotes a steric clash between the carboxylate side chain of Asp^{652} from MSR and the ribose ring of $NADP^+$. The color scheme and the residue numbering are as for Figure 5, except in panel B, the Asp^{632} residue from wild-type CPR is in magenta.

the carboxylate group of Asp^{652} when the nicotinamide group stacks against the FAD isoalloxazine ring (Figure 8B). Substitution of Trp^{677} for a glycine residue in CPR effectively removes the thermodynamic barrier for formation of the productive catalytic complex which is observed in this mutant cocrystallized with $NADP^+$. Figure 8B also shows that Asp^{632} of CPR does not move when the nicotinamide ring forms $\pi-\pi$ interactions with the isoalloxazine ring, as the residue is in the same position in both the wild-type and W677G mutant forms of CPR. Moreover, the corresponding residue in nNOS, Asp^{1385}, also superimposes with Asp^{632} of CPR, indicating that movement of the nicotinamide toward the FAD ring is also not impeded by the presence of an acidic side chain in this enzyme (data not shown).

Structural Basis for Hyperhomocysteinemia and Megaloblastic Anemia. A genetic impairment of MSR activity leads to a rare autosomal recessive disorder, and the basis for these disorders can now be analyzed from the structure of the NADP(H)/FAD module of MSR. Affected individuals present with megaloblastic anemia, hyperhomocysteinemia, and hypomethioninemia, which can lead to developmental delay, blindness, ataxia, cerebral atrophy, and neonatal seizures (*25*, *50*). Several point mutations, isolated from affected patients, have been localized to the gene encoding MSR, and residues involved in these mutations are detailed in Figure S3 of the Supporting Information. Of particular interest is an L576S substitution, as this residue is conserved among diflavin reductases. The mutation is localized in the NADPH-binding domain, on β-sheet 9, but it is unlikely to directly affect binding of the substrate as it is >14 Å from the adenine portion of the bound coenzyme. Other point mutations include C405R, G487R, and G554R. The latter mutation likely disrupts the local secondary structure as this residue is positioned within α-helix 9. As glycine residues have more conformational freedom, a mutation to arginine may cause the unusual backbone conformation of the α-helix to change at this position. Gly^{487} is close to the pyrophosphate moiety of FAD, and conversion of this residue to a bulky arginine residue is likely to affect the binding of the cofactor. Cys^{405} is located in the connecting domain near the surface of the protein and is close to Pro^{243} of the extended linker. Mutation to an arginine is likely to create clashes with neighboring residues and cause a localized change in secondary structure.

DISCUSSION

Herein we have presented a structural basis for impaired coenzyme binding to MSR relative to binding in the related protein CPR. Coupled with previous studies that (i) demonstrate MSR has a slow rate of interflavin electron transfer (*7*) and (ii) undertake a highly endergonic electron-transfer step to reduce MS (*2*), it is apparent that a number of mechanisms have evolved to attenuate catalytic turnover of MSR in the cell. Is then methionine and folate metabolism closely regulated by the ability of MSR to regenerate MS? Is MS reactivation the rate-limiting step in overall methionine synthesis? A common polymorphic variation within the MSR reading frame, which causes minor impairment of MS reactivation in vitro, yet is linked to a mild hyperhomocysteinemia phenotype (*51*), suggests that the rate of MSR turnover is critical to methionine and folate metabolism.

A Model for a Role of the MSR Flexible Extension Region in Electron Transfer. The most distinguishing structural feature of the MSR FNR module is the position of the first 31 ordered residues of the extended hinge region, as it follows a path away from the putative FMN-binding pocket. This stretch of amino acids, along with the preceding 51 residues (not shown in the structure), serves to link the connecting domain and FMN domain. The corresponding "linker" in nNOS is a small (disordered) structural element, yet it is envisioned to play an important role by enabling large-scale motion of the FMN domain so that it can serve as an electrical conduit between the FAD and the heme

acceptor (*18*, *19*). We suggest that the extended linker in MSR, which occupies an unusual position in the crystal structure, facilitates movement of the FMN domain in a similar fashion. In this capacity, the extended linker might allow MSR to mimic in part the two-component reactivation system of *Escherichia coli* cobalamin-dependent MS (MetH), a bacterial homologue of hMS. In *E. coli*, MSR function is fulfilled by two flavoproteins: an FNR-like protein that transfers NADPH-derived electrons via its FAD cofactor to the FMN redox center of flavodoxin (*6*). Reduced flavodoxin subsequently donates its electron to cob(II)alamin of MetH. NMR studies have shown that Fld forms mutually exclusive complexes with the FNR-like protein and MetH (*52*). The same binding interface on the FMN domain of MSR may also be shared between MS and the MSR NADP(H)/FAD-binding module, and the linker may facilitate movement of the FMN domain between the two.

Recent ITC studies revealed different binding stoichiometries for the binding of full-length MSR (2:1) and the isolated FMN domain (1:1) to the activation domain of MS (*2*). These data indicate that only 50% of MSR forms a complex with MS, pointing to the possibility that the enzyme may fluctuate between two conformations. For example, in one conformation (an "open" conformation) the FMN domain is amenable for interaction with MS, while in another conformation ("closed" conformation) the FMN domain is in close proximity to the NADPH/FAD-binding domain.[2] These multiple conformations would enable direct interactions with the FAD cofactor (closed conformation) and endergonic electron transfer to cob(II)alamin (open conformation). The extended and mobile linker may act to "swing" the FMN domain between the two states. This dynamic motion of the FMN domain could account for the slower rate of interflavin electron transfer observed in MSR compared to CPR (*7*, *53*, *54*). Direct interflavin electron transfer is expected to occur at a rate of 10^7 to 10^8 s^{-1} (*55*); however, in MSR the rate of electron transfer between FAD and FMN is 0.2 s^{-1} (as judged by buildup of the disemiquinone signal), and the corresponding rate in CPR is 55 s^{-1} (*53*, *54*). Interflavin electron transfer may be gated by MSR undergoing extensive conformational sampling prior to electron transfer (i.e., the FMN domain may have to search for a suitable docking site with the NADP(H)/FAD-binding module that would facilitate direct electron transfer between the FAD and FMN).

Contribution of the Adenosine and Nicotinamide Moieties in Coenzyme Binding. Extensive mutagenic and crystallographic studies have exposed the bipartite binding properties of $NADP^+$ to spinach FNR (*41*, *46*, *56*). Interpretation of binding data is assisted by visualizing the molecule split along the pyrophosphate moiety, generating nicotinamide mononucleotide (NMN) and the 2′,5′-ADP groups. For FNR and the related diflavin reductases nNOS, MSR, and CPR, the binding energy of the coenzyme is derived predominantly from the 2′,5′-ADP moiety. This is the portion of the molecule which is consistently observed in crystal structures of $NADP^+$ complexes of these proteins. In contrast, the NMN moiety is flexible and often not observed in structures, the case of nNOS being the exception. Typically the NMN group does not contribute to the coenzyme binding energy. However, in the case of FNR (5 kJ/mol) and to a greater degree MSR (7 kJ/mol), the NMN portion of the molecule contributes unfavorably to the binding energy of $NADP^+$ (*46*). The unfavorable net free energy of binding of the NMN is thought to arise from the energy lost through displacement of the aromatic residue over the *re* face of FAD (Tyr^{314} for FNR and Trp^{697} MSR), thus offsetting any favorable binding energy from NMN binding (*56*). Mutagenesis of Tyr^{314} to Ser in FNR results in a 100-fold increase in binding affinity, supporting the hypothesis that this aromatic residue destabilizes coenzyme binding (*41*). The aromatic stacking residue also appears to act in conjunction with the 2′-phosphate-binding site in selecting for the phosphorylated form of the nicotinamide, as the same mutation enhanced catalysis by NADH 1700-fold (*57*). Analogous mutations in NOS and P450 BM3 produce similar effects (*40*, *58*−*60*). In the absence of the aromatic stacking residue, either NADPH or NADH can be readily accommodated in the binding site and reduce the FAD. The role of the 2′-phosphate-binding site in discriminating between the two coenzymes in such circumstances becomes obsolete.

In contrast, the NMN group does not destabilize coenzyme binding in NOS and CPR as $NADP^+$ and 2′,5′-ADP have nearly equal binding affinities in these enzymes (*47*, *58*). Both NOS and CPR have aromatic residues stacked against the FAD, which partially blocks the nicotinamide ring from stacking against the FAD isoalloxazine ring. However, a comparison of crystal structures reveals reduced hydrophobic stacking over the isoalloxazine ring in CPR and NOS, compared to MSR. Thus, we suggest that less energy is required for movement of the corresponding aromatic residue in CPR and NOS. It seems as though CPR and NOS have retained an aromatic residue at this position to retain specificity for the coenzyme, but this residue is relatively free to move so the binding of the coenzyme is not impaired.

Prior stopped-flow studies reveal that $NADP^+$ and NADPH have similar binding constants in MSR, suggesting that the redox state of the NMN group does not significantly affect the binding affinity of the coenzyme (*7*). The binding affinity for NADPH is also likely to be significantly tighter in NOS and CPR compared to MSR as similar stopped-flow studies with these two enzymes showed that the rate of flavin reduction under pseudo-first-order conditions is unaffected by the coenzyme concentration (*54*, *61*). The higher affinity for NADPH in NOS and CPR likely allows these enzymes to fulfill their demanding physiological redox roles, i.e., the detoxification of endogenous compounds and the generation of a ubiquitous intracellular signaling molecule (NOS). By contrast, MSR needs only to turn over when MS becomes inactive (once every 200−1000 catalytic cycles of MS) and thus need not be catalytically efficient. Tight binding of NADPH to MSR and relatively fast rates of electron transfer would lead to nonproductive depletion of reduced nicotinamide coenzyme with the potential to generate unwanted reactive oxygen species. The concentration of NADPH and $NADP^+$ in human neutrophiles at least is 36 μM (*62*); however, much of the cellular nucleotide is likely to be protein-bound, so the effective cellular concentration is lower (*63*).

[2] We have also proposed, on the basis of the crystal structure of the hMS activation domain (*1*), that the difference in binding stoichiometry between the two protein complexes may represent MSR binding to the dimeric form of the activation domain (*2*).

Scheme 1

$$E + NADPH \rightleftharpoons ENADPH \rightleftharpoons E'NADPH \rightleftharpoons E + NADP^+$$

The solvent-exposed Asp^{652} located near the pyrophosphate might represent a further feature that weakens the binding of NADPH and slows the overall catalytic turnover of the enzyme. Although the residue is 4−5 Å away from the pyrophosphate in the crystal structure, electrostatic repulsion and/or steric interference may become important with rotation along the dihedral angles of the pyrophosphate bond as NADPH adopts a productive binding mode for catalysis. The position of Asp^{652} may push an equilibrium distribution of conformational states toward a nonproductive binding mode for NADPH (ENADPH, Scheme 1).

A possible consequence of the low binding affinity for NADPH is the diminished spectral signature reflecting the formation of a charge-transfer complex (E′NADPH, Scheme 1), a kinetic intermediate seen in many nicotinamide-dependent flavoproteins that represents close interaction of the nicotinamide moiety and FAD isoalloxazine ring (*7*). The reduced amount of such a species observed for the FNR module of MSR can be rationalized if multiple conformations of the enzyme−NADPH complex exist. In this case, the presence of Asp^{652} (see above) would ensure that any distribution of conformational states would be predominantly toward a nonproductive binding mode (ENADPH, Scheme 1) and thus would not contribute significant charge-transfer character during spectral analysis.

Concluding Remarks. The crystallographic structure of the FNR module of MSR provides a framework to understand the catalytic properties of MSR. The location of the hinge region supports a hypothesis in which the FMN domain adopts alternate conformations, thus allowing it to serve as an electrical conduit between the FNR module of MSR and the cob(II)alamin of MS. Compared with other diflavin oxidoreductase enzymes, subtle structural alterations within the active site weaken coenzyme binding. Compared with related diflavin enzymes, MSR is catalytically sluggish. How this impacts the mechanism of MS regeneration remains to be answered, but it is conceivable that the slow turnover of MSR (and thus MS reactivation) might be rate-limiting in methionine synthesis.

SUPPORTING INFORMATION AVAILABLE

Three figures showing the electron density of the first seven residues, the hinge region, and the ribose of FAD and a figure depicting the location of four mutations localized in individuals with a genetic deficiency in MSR activity. This material is available free of charge via the Internet at http://pubs.acs.org.

REFERENCES

1. Wolthers, K. R., Toogood, H. S., Jowitt, T. A., Marshall, K. R., Leys, D., and Scrutton, N. S. (2007) Crystal structure and solution characterization of the activation domain of human methionine synthase, *FEBS J. 274*, 738−750.
2. Wolthers, K. R., and Scrutton, N. S. (2007) Protein interactions in the human methionine synthase-methionine synthase reductase complex and implications for the mechanism of enzyme reactivation, *Biochemistry 46*, 6696−6709.
3. Olteanu, H., and Banerjee, R. (2001) Human methionine synthase reductase, a soluble P-450 reductase-like dual flavoprotein, is sufficient for NADPH-dependent methionine synthase activation, *J. Biol. Chem. 276*, 35558−35563.
4. Leclerc, D., Wilson, A., Dumas, R., Gafuik, C., Song, D., Watkins, D., Heng, H. H., Rommens, J. M., Scherer, S. W., Rosenblatt, D. S., and Gravel, R. A. (1998) Cloning and mapping of a cDNA for methionine synthase reductase, a flavoprotein defective in patients with homocystinuria, *Proc. Natl. Acad. Sci. U.S.A. 95*, 3059−3064.
5. Banerjee, R. V., Frasca, V., Ballou, D. P., and Matthews, R. G. (1990) Participation of cob(I) alamin in the reaction catalyzed by methionine synthase from *Escherichia coli*: a steady-state and rapid reaction kinetic analysis, *Biochemistry 29*, 11101−11109.
6. Fujii, K., Galivan, J. H., and Huennekens, F. M. (1977) Activation of methionine synthase: further characterization of flavoprotein system, *Arch. Biochem. Biophys. 178*, 662−670.
7. Wolthers, K. R., and Scrutton, N. S. (2004) Electron transfer in human methionine synthase reductase studied by stopped-flow spectrophotometry, *Biochemistry 43*, 490−500.
8. Massey, V., and Hemmerich, P. (1980) Active-site probes of flavoproteins, *Biochem. Soc. Trans. 8*, 246−257.
9. Warman, A. J., Roitel, O., Neeli, R., Girvan, H. M., Seward, H. E., Murray, S. A., McLean, K. J., Joyce, M. G., Toogood, H., Holt, R. A., Leys, D., Scrutton, N. S., and Munro, A. W. (2005) Flavocytochrome P450 BM3: an update on structure and mechanism of a biotechnologically important enzyme, *Biochem. Soc. Trans. 33*, 747−753.
10. Zeghouf, M., Fontecave, M., Macherel, D., and Coves, J. (1998) The flavoprotein component of the *Escherichia coli* sulfite reductase: expression, purification, and spectral and catalytic properties of a monomeric form containing both the flavin adenine dinucleotide and the flavin mononucleotide cofactors, *Biochemistry 37*, 6114−6123.
11. Iyanagi, T., and Mason, H. S. (1973) Some properties of hepatic reduced nicotinamide adenine dinucleotide phosphate-cytochrome c reductase, *Biochemistry 12*, 2297−2308.
12. Wang, M., Roberts, D. L., Paschke, R., Shea, T. M., Masters, B. S., and Kim, J. J. (1997) Three-dimensional structure of NADPH-cytochrome P450 reductase: prototype for FMN- and FAD-containing enzymes, *Proc. Natl. Acad. Sci. U.S.A. 94*, 8411−8416.
13. Bredt, D. S., Hwang, P. M., Glatt, C. E., Lowenstein, C., Reed, R. R., and Snyder, S. H. (1991) Cloned and expressed nitric oxide synthase structurally resembles cytochrome P-450 reductase, *Nature 351*, 714−718.
14. Stuehr, D. J. (1996) Purification and properties of nitric oxide synthases, *Methods Enzymol. 268*, 324−333.
15. Paine, M. J., Garner, A. P., Powell, D., Sibbald, J., Sales, M., Pratt, N., Smith, T., Tew, D. G., and Wolf, C. R. (2000) Cloning and characterization of a novel human dual flavin reductase, *J. Biol. Chem. 275*, 1471−1478.
16. Hoover, D. M., and Ludwig, M. L. (1997) A flavodoxin that is required for enzyme activation: the structure of oxidized flavodoxin from *Escherichia coli* at 1.8 Å resolution, *Protein Sci. 6*, 2525−2537.
17. Karplus, P. A., Daniels, M. J., and Herriott, J. R. (1991) Atomic structure of ferredoxin-$NADP^+$ reductase: prototype for a structurally novel flavoenzyme family, *Science 251*, 60−66.
18. Garcin, E. D., Bruns, C. M., Lloyd, S. J., Hosfield, D. J., Tiso, M., Gachhui, R., Stuehr, D. J., Tainer, J. A., and Getzoff, E. D. (2004) Structural basis for isozyme-specific regulation of electron transfer in nitric-oxide synthase, *J. Biol. Chem. 279*, 37918−37927.
19. Dunford, A. J., Rigby, S. E., Hay, S., Munro, A. W., and Scrutton, N. S. (2007) Conformational and thermodynamic control of electron transfer in neuronal nitric oxide synthase, *Biochemistry 46*, 5018−5029.
20. Bruns, C. M., and Karplus, P. A. (1995) Refined crystal structure of spinach ferredoxin reductase at 1.7 Å resolution: oxidized, reduced and 2′-phospho-5′-AMP bound states, *J. Mol. Biol. 247*, 125−145.
21. Correll, C. C., Ludwig, M. L., Bruns, C. M., and Karplus, P. A. (1993) Structural prototypes for an extended family of flavoprotein reductases: comparison of phthalate dioxygenase reductase with ferredoxin reductase and ferredoxin, *Protein Sci. 2*, 2112−2133.
22. Muller, K., Linder, D., and Lumper, L. (1990) The cosubstrate NADP(H) protects lysine 601 in the porcine NADPH-cytochrome P-450 reductase against pyridoxylation, *FEBS Lett. 260*, 289−290.
23. Sem, D. S., and Kasper, C. B. (1993) Enzyme-substrate binding interactions of NADPH-cytochrome P-450 oxidoreductase characterized with pH and alternate substrate/inhibitor studies, *Biochemistry 32*, 11539−11547.

24. Zhang, J., Martasek, P., Paschke, R., Shea, T., Siler, Masters, B. S., and Kim, J. J. (2001) Crystal structure of the FAD/NADPH-binding domain of rat neuronal nitric-oxide synthase. Comparisons with NADPH-cytochrome P450 oxidoreductase, *J. Biol. Chem. 276*, 37506−37513.
25. Wilson, A., Leclerc, D., Rosenblatt, D. S., and Gravel, R. A. (1999) Molecular basis for methionine synthase reductase deficiency in patients belonging to the cblE complementation group of disorders in folate/ cobalamin metabolism, *Hum. Mol. Genet. 8*, 2009−2016.
26. Wolthers, K. R., Basran, J., Munro, A. W., and Scrutton, N. S. (2003) Molecular dissection of human methionine synthase reductase: determination of the flavin redox potentials in full-length enzyme and isolated flavin-binding domains, *Biochemistry 42*, 3911−3920.
27. Otwinowski, Z., and Minor, W. (1997) Processing of X-ray diffraction data collected in oscillation mode, *Methods Enzymol. 276*, 307−326.
28. Navaza, J. (2001) Implementation of molecular replacement in AMoRe, *Acta Crystallogr. D57*, 1367−1372.
29. Murshudov, G. N., Vagin, A. A., and Dodson, E. J. (1997) Refinement of macromolecular structures by the maximum-likelihood method, *Acta Crystallogr. D53*, 240−255.
30. Murshudov, G. N., Lebedev, A., Vagin, A. A., Wilson, K. S., and Dodson, E. J. (1999) Efficient anisotropic refinement of Macromolecular structures using FFT, *Acta Crystallogr. D55*, 247−255.
31. Roussel, A., and Cambillau, C. (1991) TURBO-FRODO, *Silicon Graphics Geometry Partners Directory 86*, Silicon Graphics, Mountain View, CA.
32. Emsley, P., and Cowtan, K. (2004) Coot: model-building tools for molecular graphics, *Acta Crystallogr. D60*, 2126−2132.
33. Perrakis, A., Morris, R., and Lamzin, V. S. (1999) Automated protein model building combined with iterative structure refinement, *Nat. Struct. Biol. 6*, 458−463.
34. Lovell, S. C., Davis, I. W., Arendall, W. B., III, de Bakker, P. I., Word, J. M., Prisant, M. G., Richardson, J. S., and Richardson, D. C. (2003) Structure validation by Calpha geometry: phi, psi and Cbeta deviation, *Proteins 50*, 437−450.
35. van Gelder, B., and Slater, E. C. (1962) The extinction coefficient of cytochrome *c*, *Biochim. Biophys. Acta 58*, 593−595.
36. Nishida, H., Inaka, K., Yamanaka, M., Kaida, S., Kobayashi, K., and Miki, K. (1995) Crystal structure of NADH-cytochrome b_5 reductase from pig liver at 2.4 Å resolution, *Biochemistry 34*, 2763−2767.
37. Correll, C. C., Batie, C. J., Ballou, D. P., and Ludwig, M. L. (1992) Phthalate dioxygenase reductase: a modular structure for electron transfer from pyridine nucleotides to [2Fe-2S], *Science 258*, 1604−1610.
38. Lawrence, M. C., and Colman, P. M. (1993) Shape complementarity at protein/protein interfaces, *J. Mol. Biol. 234*, 946−950.
39. Shen, A. L., Sem, D. S., and Kasper, C. B. (1999) Mechanistic studies on the reductive half-reaction of NADPH-cytochrome P450 oxidoreductase, *J. Biol. Chem. 274*, 5391−5398.
40. Hubbard, P. A., Shen, A. L., Paschke, R., Kasper, C. B., and Kim, J. J. (2001) NADPH-cytochrome P450 oxidoreductase. Structural basis for hydride and electron transfer, *J. Biol. Chem. 276*, 29163−29170.
41. Deng, Z., Aliverti, A., Zanetti, G., Arakaki, A. K., Ottado, J., Orellano, E. G., Calcaterra, N. B., Ceccarelli, E. A., Carrillo, N., and Karplus, P. A. (1999) A productive $NADP^+$ binding mode of ferredoxin-$NADP^+$ reductase revealed by protein engineering and crystallographic studies, *Nat. Struct. Biol. 6*, 847−853.
42. Sem, D. S., and Kasper, C. B. (1993) Interaction with arginine 597 of NADPH-cytochrome P-450 oxidoreductase is a primary source of the uniform binding energy used to discriminate between NADPH and NADH, *Biochemistry 32*, 11548−11558.
43. Adak, S., Sharma, M., Meade, A. L., and Stuehr, D. J. (2002) A conserved flavin-shielding residue regulates NO synthase electron transfer and nicotinamide coenzyme specificity, *Proc. Natl. Acad. Sci. U.S.A. 99*, 13516−13521.
44. Newsholme, S. J., Maleeff, B. F., Steiner, S., Anderson, N. L., and Schwartz, L. W. (2000) Two-dimensional electrophoresis of liver proteins: characterization of a drug-induced hepatomegaly in rats, *Electrophoresis 21*, 2122−2128.
45. Martinez-Julvez, M., Tejero, J., Peregrina, J. R., Nogues, I., Frago, S., Gomez-Moreno, C., and Medina, M. (2005) Towards a new interaction enzyme:coenzyme, *Biophys. Chem. 115*, 219−224.
46. Batie, C. J., and Kamin, H. (1986) Association of ferredoxin-$NADP^+$ reductase with NADP(H) specificity and oxidation-reduction properties, *J. Biol. Chem. 261*, 11214−11223.
47. Grunau, A., Paine, M. J., Ladbury, J. E., and Gutierrez, A. (2006) Global effects of the energetics of coenzyme binding: NADPH controls the protein interaction properties of human cytochrome P450 reductase, *Biochemistry 45*, 1421−1434.
48. Binkowski, T. A., Naghibzadeh, S., and Liang, J. (2003) CASTp: Computed Atlas of Surface Topography of proteins, *Nucleic Acids Res. 31*, 3352−3355.
49. Munro, A. W., Noble, M. A., Robledo, L., Daff, S. N., and Chapman, S. K. (2001) Determination of the redox properties of human NADPH-cytochrome P450 reductase, *Biochemistry 40*, 1956−1963.
50. Leclerc, D., Campeau, E., Goyette, P., Adjalla, C. E., Christensen, B., Ross, M., Eydoux, P., Rosenblatt, D. S., Rozen, R., and Gravel, R. A. (1996) Human methionine synthase: cDNA cloning and identification of mutations in patients of the cblG complementation group of folate/ cobalamin disorders, *Hum. Mol. Genet. 5*, 1867−1874.
51. Olteanu, H., Munson, T., and Banerjee, R. (2002) Differences in the efficiency of reductive activation of methionine synthase and exogenous electron acceptors between the common polymorphic variants of human methionine synthase reductase, *Biochemistry 41*, 13378−13385.
52. Hall, D. A., Vander Kooi, C. W., Stasik, C. N., Stevens, S. Y., Zuiderweg, E. R., and Matthews, R. G. (2001) Mapping the interactions between flavodoxin and its physiological partners flavodoxin reductase and cobalamin-dependent methionine synthase, *Proc. Natl. Acad. Sci. U.S.A. 98*, 9521−9526.
53. Gutierrez, A., Munro, A. W., Grunau, A., Wolf, C. R., Scrutton, N. S., and Roberts, G. C. (2003) Interflavin electron transfer in human cytochrome P450 reductase is enhanced by coenzyme binding. Relaxation kinetic studies with coenzyme analogues, *Eur. J. Biochem. 270*, 2612−2621.
54. Gutierrez, A., Lian, L. Y., Wolf, C. R., Scrutton, N. S., and Roberts, G. C. (2001) Stopped-flow kinetic studies of flavin reduction in human cytochrome P450 reductase and its component domains, *Biochemistry 40*, 1964−1975.
55. Page, C. C., Moser, C. C., and Dutton, P. L. (2003) Mechanism for electron transfer within and between proteins, *Curr. Opin. Chem. Biol. 7*, 551−556.
56. Karplus, P. A., and Faber, H. R. (2004) Structural Aspects of Plant Ferredoxin : $NADP^+$ Oxidoreductases, *Photosynth. Res. 81*, 303−315.
57. Piubelli, L., Aliverti, A., Arakaki, A. K., Carrillo, N., Ceccarelli, E. A., Karplus, P. A., and Zanetti, G. (2000) Competition between C-terminal tyrosine and nicotinamide modulates pyridine nucleotide affinity and specificity in plant ferredoxin-$NADP^+$ reductase, *J. Biol. Chem. 275*, 10472−10476.
58. Dunford, A. J., Marshall, K. R., Munro, A. W., and Scrutton, N. S. (2004) Thermodynamic and kinetic analysis of the isolated FAD domain of rat neuronal nitric oxide synthase altered in the region of the FAD shielding residue Phe1395, *Eur. J. Biochem. 271*, 2548−2560.
59. Konas, D. W., Zhu, K., Sharma, M., Aulak, K. S., Brudvig, G. W., and Stuehr, D. J. (2004) The FAD-shielding residue Phe1395 regulates neuronal nitric-oxide synthase catalysis by controlling $NADP^+$ affinity and a conformational equilibrium within the flavoprotein domain, *J. Biol. Chem. 279*, 35412−35425.
60. Neeli, R., Roitel, O., Scrutton, N. S., and Munro, A. W. (2005) Switching pyridine nucleotide specificity in P450 BM3: mechanistic analysis of the W1046H and W1046A enzymes, *J. Biol. Chem. 280*, 17634−17644.
61. Knight, K., and Scrutton, N. S. (2002) Stopped-flow kinetic studies of electron transfer in the reductase domain of neuronal nitric oxide synthase: re-evaluation of the kinetic mechanism reveals new enzyme intermediates and variation with cytochrome P450 reductase, *Biochem. J. 367*, 19−30.
62. Sparkman, T. B., Johns, T., Engerson, T., and Jones, H. P. (1985) Activation-associated alterations in neutrophil pyridine nucleotide levels: a potential regulatory role for calcium and calmodulin, *Biochim. Biophys. Acta 846*, 8−13.
63. Salmon, J. M., Kohen, E., Viallet, P., Hirschberg, J. G., Wouters, A. W., Kohen, C., and Thorell, B. (1982) Microspectrofluorometric approach to the study of free/bound NAD(P)H ratio as metabolic indicator in various cell types, *Photochem. Photobiol. 36*, 585−593.

BI701209P